Biological Fate of Magnetic Protein-Specific Molecularly Imprinted Polymers: Toxicity and Degradation

Charlotte Boitard, Alberto Curcio, Anne-Laure Rollet, Claire Wilhelm, Christine Ménager, Nébéwia Griffete

The biological fate of magnetic protein-specific molecularly imprinted polymers: toxicity and degradation

Charlotte Boitard[a], Alberto Curcio[b], Anne-Laure Rollet[a], Claire Wilhelm[b], Christine Ménager[a,*], Nébéwia Griffete[a,*]

[a] Sorbonne Université, CNRS, PHysico-chimie des Electrolytes et Nanosystèmes InterfaciauX, PHENIX, F-75005 Paris, France.

[b] Laboratoire Matière et Systèmes Complexes (MSC), UMR 7057, CNRS and Université Paris Diderot, 75205 Paris Cedex 05, France.

* Corresponding authors: christine.menager@sorbonne-universite.fr ; nebewia.griffete@sorbonne-universite.fr

Abstract

Magnetic nanoparticles coated with protein-specific molecularly imprinted polymers (MIPs) are receiving an increasing attention thanks to their binding abilities, robustness and easy synthesis compared to their natural analogues also able to target protein, such as antibodies, or aptamers. Acting as tailor-made recognition systems, protein-specific molecularly imprinted polymers can be used in many *in vivo* nanomedicine applications, such as targeted drug delivery, biosensing and tissue engineering. Nonetheless, studies on their biocompatibility and long-term fate in biological environments are almost non-existent, although these questions have to be addressed before considering clinical applications. To alleviate this lack of knowledge, we propose here to monitor the effect of a protein-specific molecularly imprinted polymer coating on the toxicity and biodegradation of magnetic iron oxide nanoparticles, both in a minimal aqueous degradation medium and in a model of cartilage tissue formed by differentiated human mesenchymal stem cells (MSC). Iron oxide nanoparticles degradation with or without the polymer coating was monitored for a month by following their magnetic properties using vibrating sample magnetometry, and their morphology by transmission electron microscopy. We showed that the MIP-coating of magnetic iron oxide nanoparticles do not affect their biocompatibility or internalization inside cells. Remarkably, the imprinted polymer coating does not hinder the magnetic particles degradation, but seems to slow it down, although this effect is more visible when degradation occurs in the buffer medium than in cells. Hence, the results presented in this paper are really encouraging and open up the way to future applications of MIP-coated nanoparticles into the clinic.

Keywords: imprinted polymer; iron oxide nanoparticles; toxicity; degradation; stem cells

Introduction

Protein-specific molecularly imprinted polymer (MIP) particles have unique physical and chemical properties allowing them to specifically bind a define biomolecule. They are an innovative, cheap and robust alternative to their natural counterparts such as antibodies, aptamers[1,2] or chromobodies[3,4] when protein targeting is required. Indeed, these molecules are difficult to obtain, often depending on either animal hosts[5,6] or time-consuming synthetic pathways[7,8]. In the meantime, MIP can be produced by simply polymerizing functional monomers in presence of template proteins. After template removal, cavities perfectly complementary to the target biomolecule in terms of size, shape and interaction points remain[9]. They are the so-called protein-specific imprints. Over the past few years, numerous synthetic pathways were developed to produce them[10–12], and interest recently focused on their potential applications for biomedicine. Among remarkable applications, growth factors were imprinted either to increase the selectivity of a drug-delivery platform[13] or to simply entrap them and thus acting as an inhibition system[14]. Another interesting system having biomedical applications was recently developed by coupling an imprinted polymer to maghemite nanoparticles (γ-Fe_2O_3) and taking advantage of their hyperthermia properties to actively release entrapped drugs[15]. Indeed, when submitted to an alternative magnetic field, magnetic iron oxide nanoparticles will dissipate energy as heat and thus locally increase temperature[16,17], leading to the breaking of hydrogen bonds between molecules and polymer. It must be underlined that these nanoparticles also have other interesting properties, such as being employed as contrast agents in magnetic resonance imaging[18].

However, the biocompatibility and long-term fate of protein-specific imprinted nano-objects remain unknown. To the best of our knowledge, only a small amount of paper deals with the toxicity of imprinted polymer[13,14,19–21], but none records the effect of magnetic MIP on cell survival or its degradation in a bio-environment. Considering their potential applications for protein targeting and

inhibition, these information are mandatory to predict their clinical safety and consider their medical applications.

The objective here was thus to palliate this lack of data, by studying the effect of an imprinted polymer coating on the toxicity and degradation of magnetic iron oxide nanoparticles, well referenced in the literature[18,22,23]. To do so, we synthesized γ-Fe_2O_3@MIP nano-objects using a "grafting from" polymerization approach and assessed the effective synthesis of the imprinted polymer coating. Magnetic nanoparticles transformation was then monitored over time under conditions of increasing complexity. The first one was a minimal biomimetic degradation medium, namely an aqueous acidic buffer solution containing iron chelating molecules to mimic lysosomal environment, as it is now a common observation that most nanomaterials interacting with cells end up confined in intracellular compartments, the lysosomes[24,25]. After assessing the cytotoxicity of the particles, their degradation in a model tissue being a spheroid of human mesenchymal stem cells was monitored[26,27]. The degradation kinetics was determined using the loss of magnetic properties during iron oxide nanoparticles dissolution, and confirmed by transmission electron microscopy.

Materials and methods

Chemicals

Sodium citrate, pronase, glucosidase, lysozyme, PBS, dexamethasone, sodium pyruvate, 2-phosphate ascorbic acid, L-proline, RPMI (Roswell Park Memorial Institute), FBS (fetal bovine serum), Penicillin-Streptomycin, glutaraldehyde, and Epon were provided by Sigma. DMEM (Dulbecco's modified Eagle medium) and trypsin were purchased at Gibco. Citric acid was provided by Carlo Erba, chlorhydric acid (37%) by Merck, nitric acid (68%) by VWR, MSCBM (Mesenchymal Stem Cell Basal Medium) by Lonza, ITS Premix by BD Biosciences, TGF-β_3 by Oncogene, PC3 cells (Human prostate

adenocarcinoma) ATCC®CRL-1435™, AlamarBlue by Invitrogen, uranyl acetate by Fisher Scientific and human mesenchymal stem cells (MSC) originated from bone marrow donations.

Magnetic nanoparticles and hybrid nano-objects

Maghemite nanoparticles and magnetic imprinted polymers were prepared and characterized following a synthetic protocol previously described[28] (see Supporting Information).

Lysosome-like buffer solution

In vitro degradation experiments were carried out in 20mM citric acid at pH=4.55. The citrate buffer was prepared by mixing 4.4mM of citric acid ($C_6H_8O_7$, Carlo Erba) and 5.6mM of sodium citrate tribasic ($C_6H_5Na_3O_7.2H_2O$, Sigma-Aldrich) in 500mL of purified water. Some experiments were also performed in a lysosome-like buffer solution modified with glucosidase (Sigma) at 0.5mg/mL.

Cell culture and nanoparticles internalization

Human mesenchymal stem cells (MSC, from bone marrow donations) were cultured until 90% confluence in T75 flasks at 37°C with 5% CO_2 in mesenchymal stem cells basal medium (MSCBM) (Lonza). They were labelled with bare and MIP-coated maghemite nanoparticles for 30 minutes at the iron concentration of 0.05, 0.1 and 0.2 mM in serum-free Dulbecco's modified Eagle medium (DMEM, Gibco). At the end of the labelling the cells were rinsed with serum-free DMEM and then incubated in complete MSCBM for 3 hours chasing in order to get rid of any particles stuck on the cells membrane.

Spheroid formation and maturation

After incubation with the various nanoparticles, the cells were detached by means of trypsin-EDTA solution (Gibco). Cells were counted, centrifuged and suspended in specific (chondrogenic-like)

media for spheroid formation, composed of serum-free DMEM containing dexamethasone (Sigma Aldrich, final concentration 0.1 µM), sodium pyruvate (Sigma Aldrich, final concentration 1 mM), ascorbic acid-2 phosphate (Sigma Aldrich, final concentration 50 µM), L-proline (Sigma Aldrich, 0.35 mM), ITS Premix (BD Biosciences, 1/100 dilution) and TGF-β_3 (Oncogene, final concentration 10 ng/mL). The cells were divided in several suspensions of same cell number (220 000 cells in 15 mL tubes), centrifuged at 1200 rpm for 4 minutes and placed at 37°C. After 24 hours, the pellets started to shrink and form a three-dimensional cellular spheroid with tissue-like features. The medium was renewed every 3-4 days. At day 0, 3, 9 and 21 of maturation, the spheroids were collected, fixed in 5% glutaraldehyde and kept in phosphate-buffered saline (PBS, Sigma) for further characterization (VSM and electron microscopy imaging).

Alamar Blue test

Human prostate adenocarcinoma PC3 cells (ATCC® CRL-1435™) were cultured in Dulbecco's Modified Eagle's Medium (DMEM high glucose, Gibco) supplemented with 10% Fetal Bovine Serum (heat inactivated FBS) and 1% Penicillin-Streptomycin (5000 U/mL) at 37°C with 5% CO_2. Patient-derived mesenchymal stem cells (MSC) were cultured until 90% confluence in T75 flasks at 37°C with 5% CO_2 in complete MSC Basal Medium (MSCBM, Lonza). Cells were plated ($2x10^5$ PC3 and $0.5x10^5$ MSC per well) in 48 multi-well culture plates 24 hours prior to the incubation with the nanohybrids. Bare and MIP-coated maghemite nanoparticles, corresponding to 15, 62 and 250 µM of Fe, were dispersed in serum free RPMI medium at the concentration of 0.05, 0.1 and 0.2 mM of Fe and incubated with cells for 30 min. As control, non-magnetic MIP (see SI for experimental data on their synthesis) was also incubated at the equivalent concentration corresponding to 6.1, 12.2 and 24.4 µg/mL of polymer. At the end of the incubation, the cells were thoroughly washed 3 times with PBS and incubated with their respective complete media. After 24h, the metabolic activity was measured using the Alamar blue reagent (Invitrogen). After one PBS rinsing, cells were incubated with Alamar Blue solution (10% in serum-free DMEM) without phenol red for 2h. Then this medium was transferred in 96 well plates

and their fluorescence due to the reduction of resazurin (oxidized form) to resorufin by cell activity was quantified with a microplate reader (excitation 570 nm, emission 585 nm). The results were normalized with respect to untreated controls in same conditions. All measurements were performed in quadruplicate.

Free iron concentration determination

At each time point during degradation, 1 mL of lysosome-like buffer solutions containing bare or MIP-coated magnetic nanoparticles was filtered to remove non-dissolved nanoparticles from the liquid solution containing the free iron (originating from the dissolved nanoparticles). The iron concentration [Fe] of these solutions was determined by atomic absorption spectroscopy using a Perkin Elmer Analyst 100 system after dilution with filtered ultrapure water (in 2% HNO_3, VWR). Measurements were performed in triplicate.

Magnetic measurements

At each time point, fixed spheroids were introduced in sample capsules for vibrating sample magnetometry (VSM) analysis (Quantum Design, Versalab). Field-dependent magnetization curves were measured at 300 K as a function of the external field, in the range 0 to 3 T (step rate of 30 mT/s) to obtain saturation magnetization and in the range of −150 to +150 mT, with a step rate of 10 mT/s, for more precise measurements. The magnetic moment thus recorded (in emu) can directly be converted into grams of iron per spheroid, due to the magnetization at saturation of each material (expressed in emu/g of iron). Measurements were performed in triplicate.

Analysis of magnetization curves: log-normal size distribution of the nanoparticles

The magnetization curve M(H) of a suspension of monodisperse iron oxide nanoparticles can be described by a Langevin formalism:

$$M(H) = m_s\phi(coth\,\xi - \frac{1}{\xi})\ (1)$$

where $\xi = \mu_0 m_s VH/kT$ is the Langevin parameter, μ_0 the vacuum magnetic permeability, m_s the saturation magnetization of the magnetic material, H the magnetic field, k the Boltzmann constant, T the temperature, V the particle's magnetic volume, and φ the volume fraction of particles in the suspension. For a polydisperse sample, M(H) can be adjusted by weighting the Langevin expression by a log-normal distribution of particle diameter d:

$$P(d) = \frac{1}{\sqrt{2\pi}\sigma d}\exp\left(-\frac{ln^2(\frac{d}{dmag})}{2\sigma^2}\right)\ (2)$$

and the fit of the magnetization curves by eq. 1 combined with eq. 2 leads to the mean magnetic diameter d_{mag} and the polydispersity index σ.

NMR relaxation time measurements

NMR transverse relaxation times T_2 of bare and MIP coated magnetic nanoparticles in lysosome-like buffer solutions were recorded on a Minispec mq20, BRUKER at 20MHz and 25°C. T_2 were measured using a CPMG sequence[29,30] with 4 scans of 500 echoes separated by 40 µs and 5 s recycle delay. Magnetization decay was mono-exponential and measurements were performed in triplicate.

Transmission Electron Microscopy

The TEM analysis of bare nanoparticles and hybrid nano-objects was performed using a JEOL-100 CX TEM, while high resolution transmission electron microscopy (HRTEM) was performed on a JEOL 2100F microscope. A droplet of diluted nanoparticles suspension in water was deposited on a carbon coated copper grid and the excess was drained using a filter paper. Size analysis was achieved on TEM images using ImageJ software.

The spheroids used for TEM were fixed for 1 h at room temperature with 5% glutaraldehyde in 0.1 M cacodylate solution, and included in Epon resin after dehydration. Slices 70 nm thick were colored using uranyl acetate and observed with a Phillips Tecnai 12 electron microscope.

X-ray Diffraction

X-ray diffractograms were recorded using a PANALYTICAL X'pert Pro MPD diffractometer with the Cu K_α radiation (K_α = 1.54 Å).

Statistical analysis

All values are reported as means and standard deviation (error bars). Student-t test (unpaired) was used to determine whether results were significantly different. A confidence level of 95% was considered significant; *** corresponds to $p<0.001$, ** to $p<0.01$ and * to $p<0.05$.

Results and discussion

While biocompatibility and intracellular degradation of iron oxide nanoparticles have been extensively monitored in the past few years[31–33], no study highlighted the effect of the polymer. This coating being extremely porous to allow the diffusion and adsorption of proteins, it should not hinder degradation of hybrid nano-objects magnetic core but it remained to be proved. In order to assess the influence of imprinted polymer coatings on magnetic nanoparticles degradation, we chose to work with magnetic GFP-imprinted polymer nanoparticles, also called γ-Fe_2O_3@MIP, GFP being the green fluorescent protein. This protein was chosen because it is not expected to be present in the cells or in the culture media, so the effects observed will only be due to the presence of the imprinted polymer and not to the binding of particles to any cellular structure.

Imprinted nano-objects (Figure 1A) were synthesized according to a method described in a previous publication[28]. Briefly, γ-Fe_2O_3 nanoparticles were produced using a co-precipitation method, followed by an oxidative step. Particles were then functionalized to ensure their coupling with the imprinted polymer, formed using a controlled radical polymerization (see SI for experimental details). The obtained nano-objects are composed of a magnetic core made of several maghemite nanoparticles

and an imprinted polymer shell. Transmission electron microscopy (TEM) displays what seemed to be aggregates of magnetic nanoparticles, with a size ranging from 100 nm to 200 nm (Figure 1, B1 and B2). Aggregation of maghemite can be related to the poor solubility of the functionalizing agent in aqueous media, hence leading to a poor stability of the functionalized-particles suspension. High-resolution TEM evidences an amorphous coating around these aggregates identified as the polymer coating (Figure 1 B3). Infra-red Fourier transform spectroscopy and thermogravimetric analysis confirms this amorphous phase to be the polymer coating (see Figure S1, ESI†). Coating thickness varied between 1 nm and 10 nm as measured on TEM images (Figure 1 B3), which is enough to potentially contain imprints, green fluorescent proteins having a size of approximatively 4.2 nm x 2.4 nm[34]. Imprints presence was assessed using a rebinding experiment as extensively described in the literature[35,36]. This experiment showed that γ-Fe_2O_3@MIP nano-objects were able to adsorb more than twice the quantity of proteins than their non-imprinted counterparts, demonstrating the effectiveness of the imprinting process.

Finally, magnetometry measurements using a vibrating sample magnetometer were performed to prove that γ-Fe_2O_3@MIP nano-objects were able to respond to magnetic field (see Figure S1C, ESI†). The imprinted polymer does not hinder the magnetism of the maghemite nanoparticles[37], and characterization methods based on this property could be applied to follow iron oxide degradation.

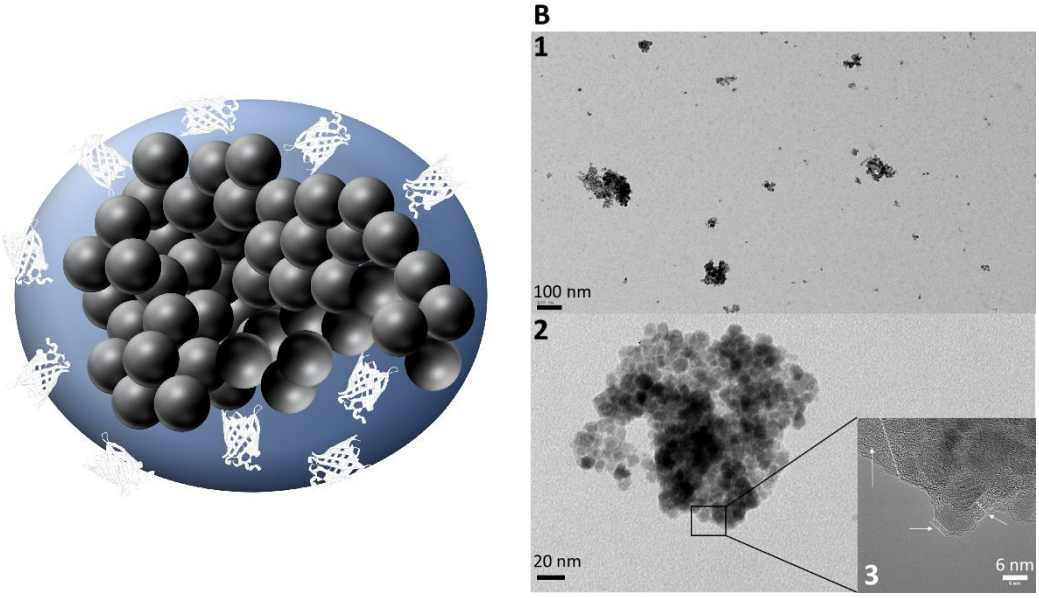

Figure 1: Description of magnetic imprinted polymers used in this study. (A) Schematic representation of the synthesized nano-objects. The black spheres represent iron oxide magnetic nanoparticles (γ-Fe_2O_3) embedded inside the polymer matrix (blue). The white shadows stand for the protein imprints, being either two-dimensional on the surface or three-dimensional inside the polymer. (B) Transmission electron microscopy of magnetic imprinted polymers with different magnification. B1: scale bar: 100nm, B2: scale bar 20 nm, B3: high-resolution TEM, scale bar: 6 nm. Polymer coating thickness varied between 1 nm and 10 nm.

Nano-objects degradation within the lysosome-like buffer solution

Before working in a highly complex medium being a model tissue composed of human mesenchymal stem cells, degradation of magnetic nanoparticles embedded inside an imprinted polymer was first assessed in a lysosome-like buffer medium, being an aqueous buffer medium at pH=4.7 containing citrate ions to mimic iron chelating agents.

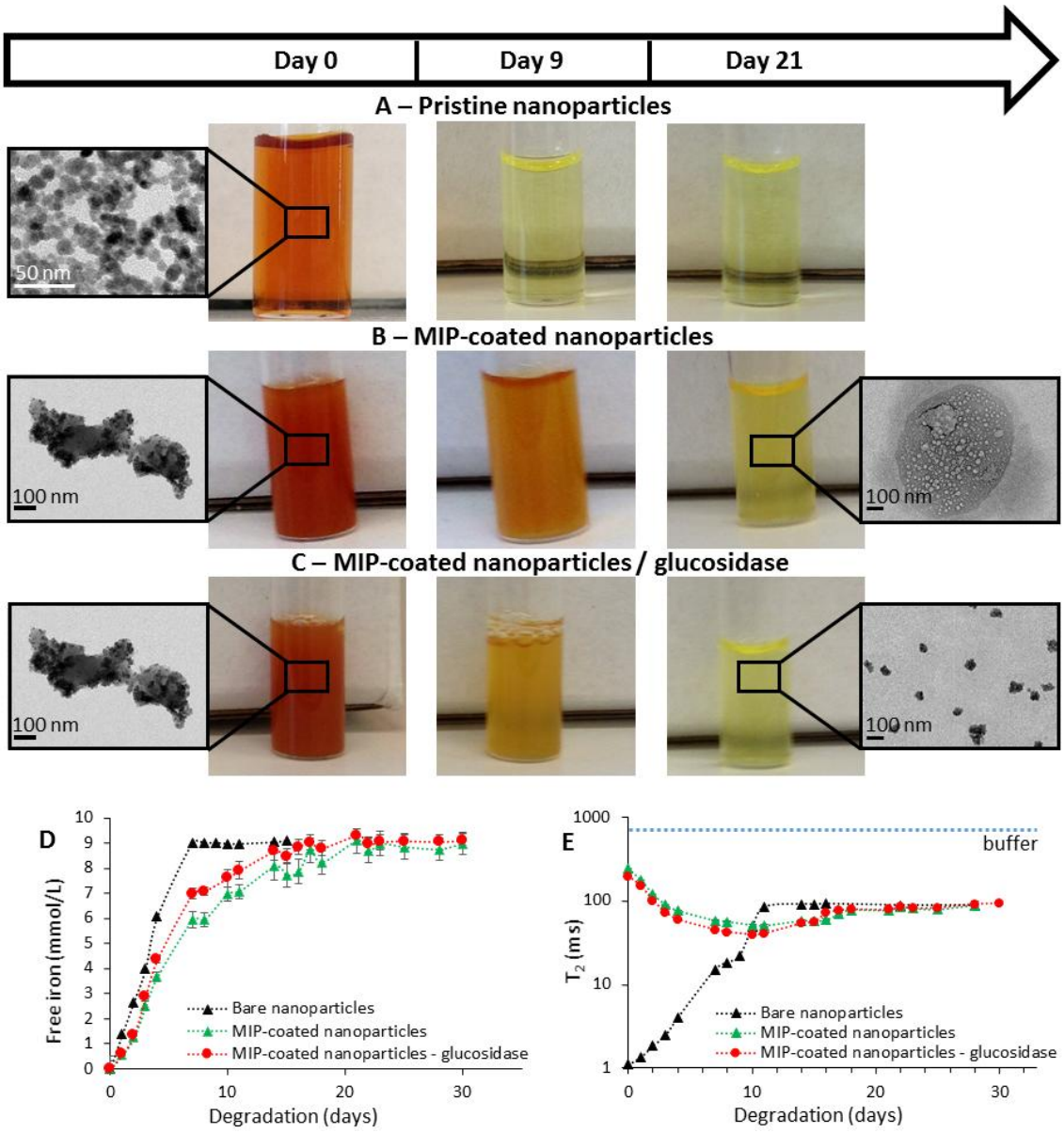

Figure 2: Degradation of hybrid nano-objects in lysosome-like buffer solution. (A) Camera images of maghemite nanoparticles dispersed in the buffer during degradation. From day 0 to day 21, nanoparticles are dissolved by the medium resulting in a change of the dispersion color. Transmission electron microscopy of the dispersion on day 0 is shown as inset (scale bar 50 nm). (B, C) Camera images of γ-Fe_2O_3@MIP nano-objects dispersion in lysosome-like buffer solution containing (C) or not (B) a glucosidase enzyme, during degradation from day 0 to day 21. Transmission electron microscopy of the nano-objects in the different buffer at the beginning and the end of the degradation are shown as inset (scale bar 100 nm). (D) Free iron concentration in the lysosome-like buffer medium over time. (E) NMR transverse relaxation time during degradation.

The kinetic of iron oxide nanoparticles transformation was assessed in the lysosome-like buffer medium proposed by Arbab *et al.*[38] using several analytical methods, such as free iron concentration determination, TEM imaging and NMR transverse relaxation time measurements. Pristine or MIP-

coated iron oxide nano-objects were immerged in the buffer medium for a month and the nanoparticles evolution was probed at various time.

In the lysosome-like medium, maghemite transformation was synonymous to their complete dissolution. Indeed, color of particles suspensions changed over time, from the dark orange characteristics of maghemite nanoparticles, to a pale yellow corresponding to a solution of ionic iron (see Figure 2A, B and C). Note that suspensions of MIP-coated nano-objects are darker and more turbid than the one of pristine nanoparticles due to the presence of the polymer. Objects are therefore bigger and polymer will scatter light differently than bare iron oxide, opacifying the solution. Interestingly, polymer coating seems to be able to slow down the degradation process of iron oxide nanoparticles, as at least 21 days are needed to induce a complete change of color, while only 9 days are needed for bare nanoparticles. A macroscopic following of the suspensions thus highlights the degradation of the magnetic nanoparticles, but a more thorough follow-up is needed to assess its mechanism, and microscopic analysis are carried out.

Morphology of different hybrid nano-objects was monitored during degradation using transmission electron microscopy. Suspensions were observed at day 1 and day 21. Without enzyme, MIP-coated particles with a mean diameter between 500 nm and 750 nm are observed both at the beginning and the end of the immersion in the lysosome-like buffer medium, as displayed in the inset on Figure 2B. Polymer was not affected by the degradation medium, which is confirmed by the absence of significant evolution of the nano-objects mean size (see Figure S2, ESI†). Small holes with a mean diameter of approximatively 10 nm are clearly visible on TEM images of MIP-coated nano-objects after 21 days in the lysosome-like medium. This holes are the cavities left by the maghemite nanoparticles inside the polymer matrix, corroborating the hypothesis of their dissolution. In the presence of glucosidase, one can observe small polymeric particles without maghemite inside, 21 days after the beginning of the degradation (TEM image on Figure 2C). This observation, coherent with the recorded evolution of the nano-objects mean size, evidence the role of enzymes (see Figure 2C and Figure S2, ESI†). Glucosidase is able to cleave the polymer, facilitating access to nanoparticles

surface for chelating agent, and therefore explaining the faster color change of the suspension. Note that mean hydrodynamic diameter of pristine nanoparticles showed no significant evolution, suggesting an all-or-nothing degradation mechanism[26].

Evolution of free iron concentration in the degradation media confirmed the nanoparticles dissolution over time, as concentration reached a plateau of 9 mM, equivalent to the initial iron concentration in nanoparticles, as displayed on Figure 2D. Indeed, at the beginning all iron was contained inside the maghemite nanoparticles. During their dissolution, iron is chelated by degradation agents and freed in the lysosome-like medium, therefore increasing the free iron concentration[39,40]. The increase of free iron concentration being slower for solutions containing MIP-coated nanoparticles than for the one containing only pristine maghemite nanoparticles, it evidenced the influence of the polymer. Nevertheless, the dissolution is not completely hindered by the MIP coating revealing that the polymer is porous enough to allow solvent accessing the nanoparticles surface. The dissolution of maghemite nanoparticles seems a little faster when glucosidase is present in the degradation medium as both revealed by NMR relaxometry and free iron concentration measurements (see Figure 2D and E, red and green curves). The enzyme, by cleaving the imprinted polymer, facilitates the access of degrading agent to the iron oxide nanoparticles surface and consequently the dissolution of the latter.

The superparamagnetism of iron oxide nanoparticles induces a great enhancement of the NMR relaxation[41–43], due to dipolar interactions between particles and ^{1}H protons. During the degradation of maghemite nanoparticles, NMR transverse relaxation time (T_2) will be both influenced by magnetic nanoparticles concentration and size and by free iron concentration. The NMR T_2 of coated nanoparticles decreased to reach a plateau (100 ms) after approximately 18 days while for the bare nanoparticles, the T_2 increased (Figure 2E). The behavior difference is due to the difference of accessibility of the water to the relaxing agent (i.e. nanoparticle or iron ion). Indeed, the dipolar interaction responsible of the NMR relaxation has an $1/r^3$ dependence, where r is the distance between ^{1}H protons and superparamagnetic nanoparticles[41,43–45]. The polymer corona hinders

without preventing the water diffusion at the vicinity of the maghemite nanoparticles by modifying the minimal approach distance of water to nanoparticles whereas no barrier exist for bare nanoparticles or free iron ions[46–49]. At this magnetic field and for a given total amount of iron, the relaxivity order is bare nanoparticles >> free iron ion > MIP-coated nanoparticles (note that the buffer T_2 is equal to 2000 ms). Hence, T_2 increases upon degradation in the case of bare nanoparticles, and T_2 decreases in the case of MIP-coated nanoparticles. Interestingly, the value of the plateau is the same for all samples demonstrating that the degradation is complete for all and that the MIP-coating has no influence of the final degradation state.

Study of nano-objects degradation within the lysosome-like buffer solution thus suggests that the different accessibility of iron chelating agent to iron oxide nanoparticles surface, tuned through the presence of polymer coating and glucosidase enzyme, will impact degradation kinetics without hindering it.

Nano-objects cytotoxicity assessment using a cell viability assay

As we hope for γ-Fe_2O_3@MIP nano-objects to be internalized by cells, their short-time cytotoxicity has to be assessed in vitro using a toxicological test, before forming spheroids and allowing them to mature for up to 21 days. The biocompatibility of magnetic imprinted polymer nano-objects was evaluated in prostatic cancer cells (PC3) and human mesenchymal stem cells (MSC). PC3 were chosen as a model of tumor-derived cell line, and mesenchymal stem cells were chosen as a model of normal (non-tumoral) primary culture. The MSC are a very good biocompatibility benchmark because they are very sensitive to any toxic extracellular perturbation.

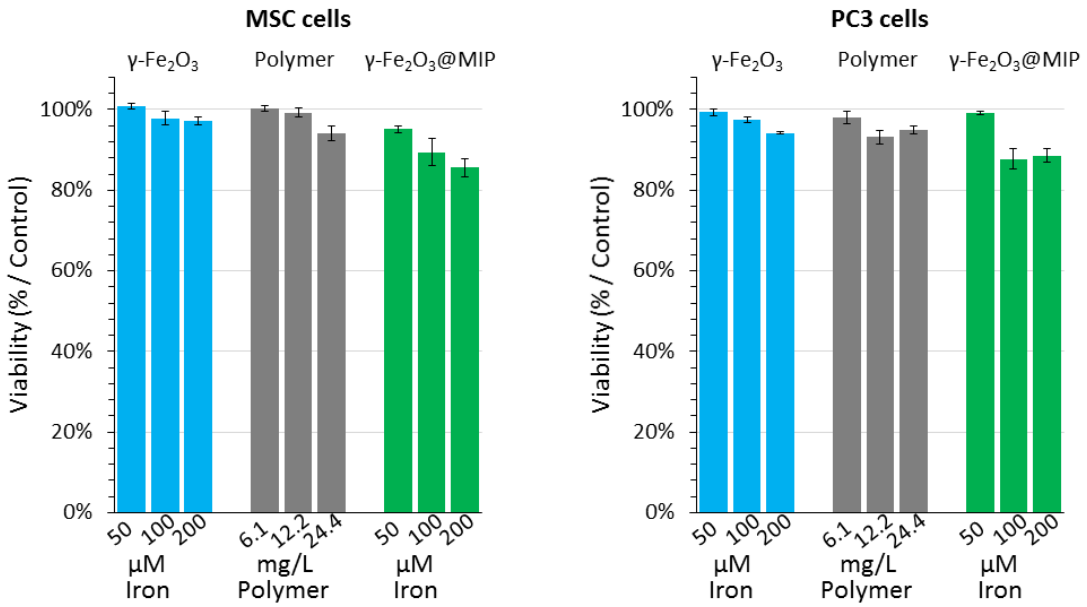

Figure 3: Cell viability assay (AlamarBlue test) performed on both MSC and PC3 cells.

The AlamarBlue assay used as cell viability test relies on the measurement of the fluorescent pink product (resorufin) formed after reduction of the blue compound resazurin by mitochondrial dehydrogenase. Therefore, its activity adequately reflects the metabolic activity of the cells that could be affected by the presence of foreign hybrid nano-objects in the cellular media. Three concentrations of γ-Fe_2O_3@MIP nano-objects were incubated with both MSC and PC3 cells (equivalent in iron: 0.05, 0.1 and 0.2 mM / equivalent in polymer: 6.1, 12.2, 24.4 mg/mL), and in the same way, equivalent concentrations of iron nanoparticles and non-magnetic polymer nanoparticles were tested, while non-treated cells served as control. As displayed on Figure 3, after 24h the metabolic activity of both cell lines was only slightly affected by the magnetic imprinted polymers, as the γ-Fe_2O_3@MIP nano-objects did only show a cytotoxicity between 10-15% at the concentrations tested. The low cytotoxicity both of the maghemite nanoparticles and the imprinted polymer alone are both displayed, and coherent with what is already described in the literature[22,23,50,51].

Overall, these results confirm the high biocompatibility of the hybrid nano-objects and are promising for their future translation in the clinic. Furthermore, the low cytotoxicity of pristine and MIP-coated nano-objects on MSC cells, validate the next results regarding their long-term degradation.

Nano-objects internalization by mesenchymal stem cells

The next challenge was to assess iron oxides degradation in a more complex biological medium. Spheroids of mesenchymal stem cells were recently developed as a model tissue to monitor intracellular bio-transformations of nano-objects[26,27,52,53]. We thus chose this tissue-like model to determine whether the imprinted polymer coating impacted degradation of maghemite nanoparticles. To do so, we first evaluated the internalization of γ-Fe_2O_3@MIP nano-objects and the subsequent spheroid formation.

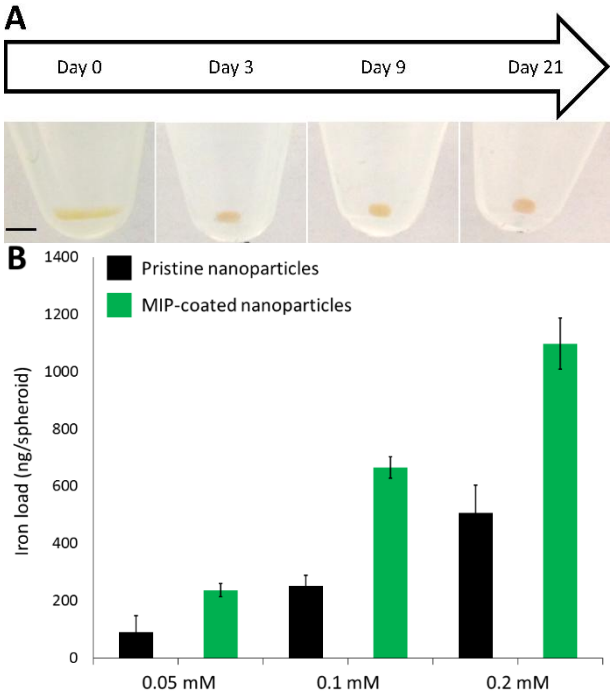

Figure 4: Nano-objects internalization and spheroids formation. (A) Camera images of the formation and maturation of a single representative spheroid. From day 0 to day 21, the spheroid matures and rounds up (scale bar: 2 mm, same on all images). (B) Iron load of spheroids formed after internalization of bare or MIP-coated maghemite nanoparticles incubated at different initial iron concentrations ([Fe] = 0.05, 0.1 and 0.2 mM).

Camera images of the spheroid formation and maturation process are displayed on Figure 4. On the first maturation days, the cell pellet obtained after centrifugation compacts and rounds up to form a spheroid, as already reported[26,52,53], which is also indicative that the nanoparticles do not interfere with the stem cell adhesion and maturation processes. Single spheroids magnetic moment could then be measured by magnetometry, using a vibrating sample magnetometer, on the day of spheroid formation. These magnetic moments directly relate to the spheroids magnetic iron load (in the µg

range). Three initial iron concentrations (0.05, 0.1 and 0.2 mM) and two types of particles (pristine and MIP-coated maghemite nanoparticles) were tested with stem cells. All conditions led to an effective internalization of nano-objects by cells as all spheroids displayed an iron load over 100 ng (see Figure 4B) and up to 1 µg, increasing with the initial nanoparticles concentration during incubation.

Interestingly, MIP-coated nanoparticles entered more efficiently inside cells. Indeed, the same initial maghemite concentration lead to an iron load almost two-times higher for the coated nano-objects. As interest focused on the effect of the polymer-coating on magnetic iron oxide degradation, we chose to compare nanodegradation within spheroids with same iron load, that is corresponding to an initial iron concentration of 0.1 mM for pristine nanoparticles and 0.05 mM for MIP-coated nano-objects.

Follow-up of magnetic properties of nano-objects during maturation of spheroids

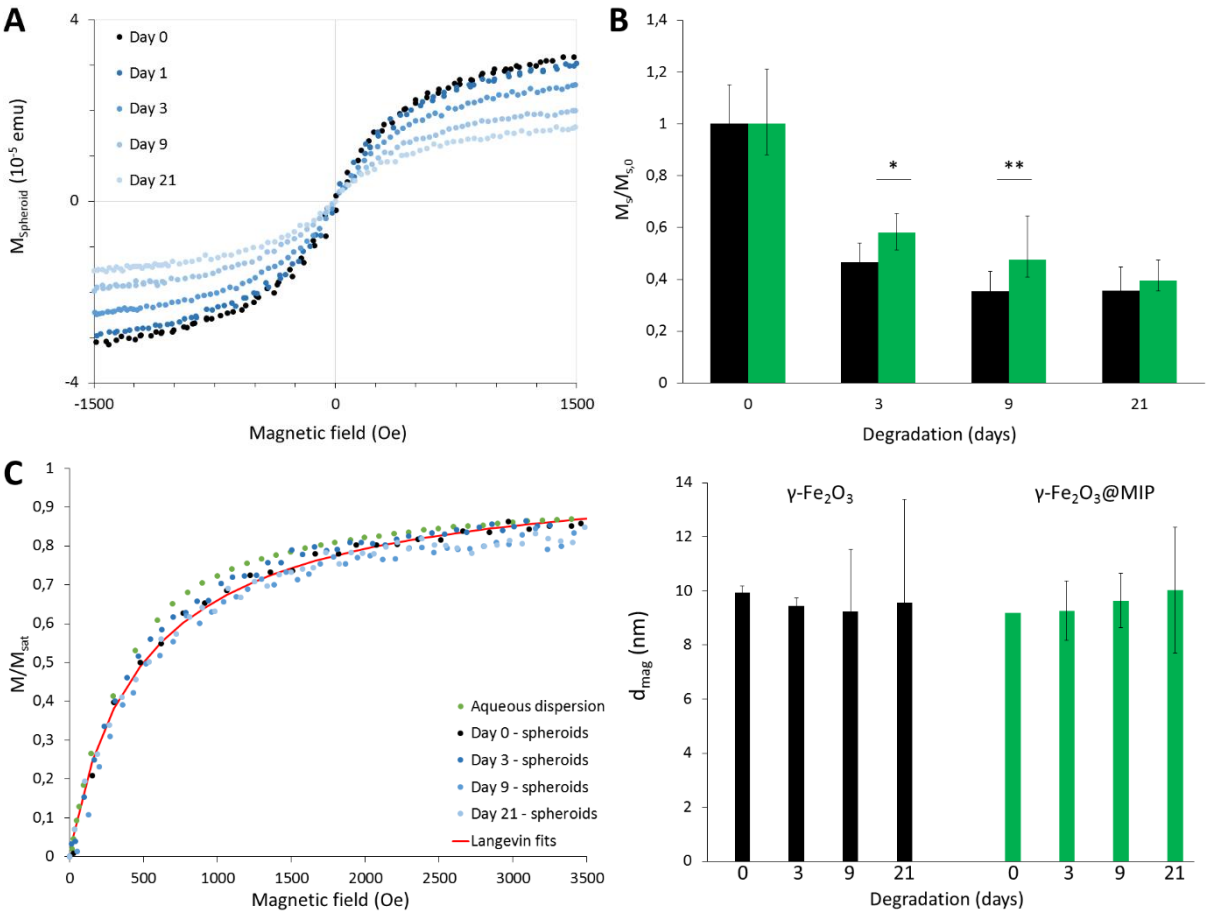

*Figure 5: Magnetic follow-up of the maghemite nanoparticles (bare and MIP-coated) degradation process in the model tissue. (A) Typical vibration curves obtained for a single spheroid on different days after spheroid formation using a vibrating sample magnetometer. These particular curves were obtained with spheroids having internalized MIP-coated nanoparticles. (B) Evolution of the saturation magnetization (normalized by its initial value) over time of spheroids after internalization of bare or MIP-coated maghemite nanoparticles. Student's t-test was performed each day between the values obtained for bare and MIP-coated particles (*corresponds to p<0.05 and ** indicates p<0.01). (C) Renormalized magnetization curves (left) obtained for the nanoparticles in spheroid at day 0 or day 21. Curves are quasi-identical and can be fitted by a Langevin law pondered by log-normal size distribution (see Materials and methods for the equations). Analysis of each curve provided the mean magnetic diameter d_{mag} of the maghemite nanoparticles (right plot) and the polydispersity index σ (shown in ESI, Figure S4).*

The very small size of spheroids makes it impossible to measure reliable NMR relaxation times with standard NMR relaxometer (see Figure S3, ESI[†]). By contrast, magnetometry is sensitive enough to monitor the spheroids magnetization decrease over tissular nanodegradation. All single spheroids magnetic moments were thus measured at different times of tissue maturation (days 0, 3, 9, and 21). Typical magnetization curves obtained for a single spheroid on different days are displayed on Figure 5A. The spheroid magnetic moment, retrieved from these curves, clearly collapsed over time, losing 60% to 65% of its initial value depending on the nature of the internalized nanoparticles (see Figure 5B). It is noteworthy to mention that the imprinted polymer coating slowed down the spheroid magnetic moment decrease, but did not hinder it, probably due to its high porosity.

From the magnetization curves, one can also retrieve the size distribution of nanoparticles within the sample. Renormalized spheroid magnetization curves on different days after their formation displayed the same allure (see Figure 5C) and could be fitted using the Langevin formalism as explained in Materials and Methods, equations 1 and 2. This indicates that the nanoparticle size distribution was not affected by the degradation, validating the all-or-nothing degradation mechanism proposed in previous works[26].

Long-term imaging of bare and MIP-coated nanoparticles within the model tissue

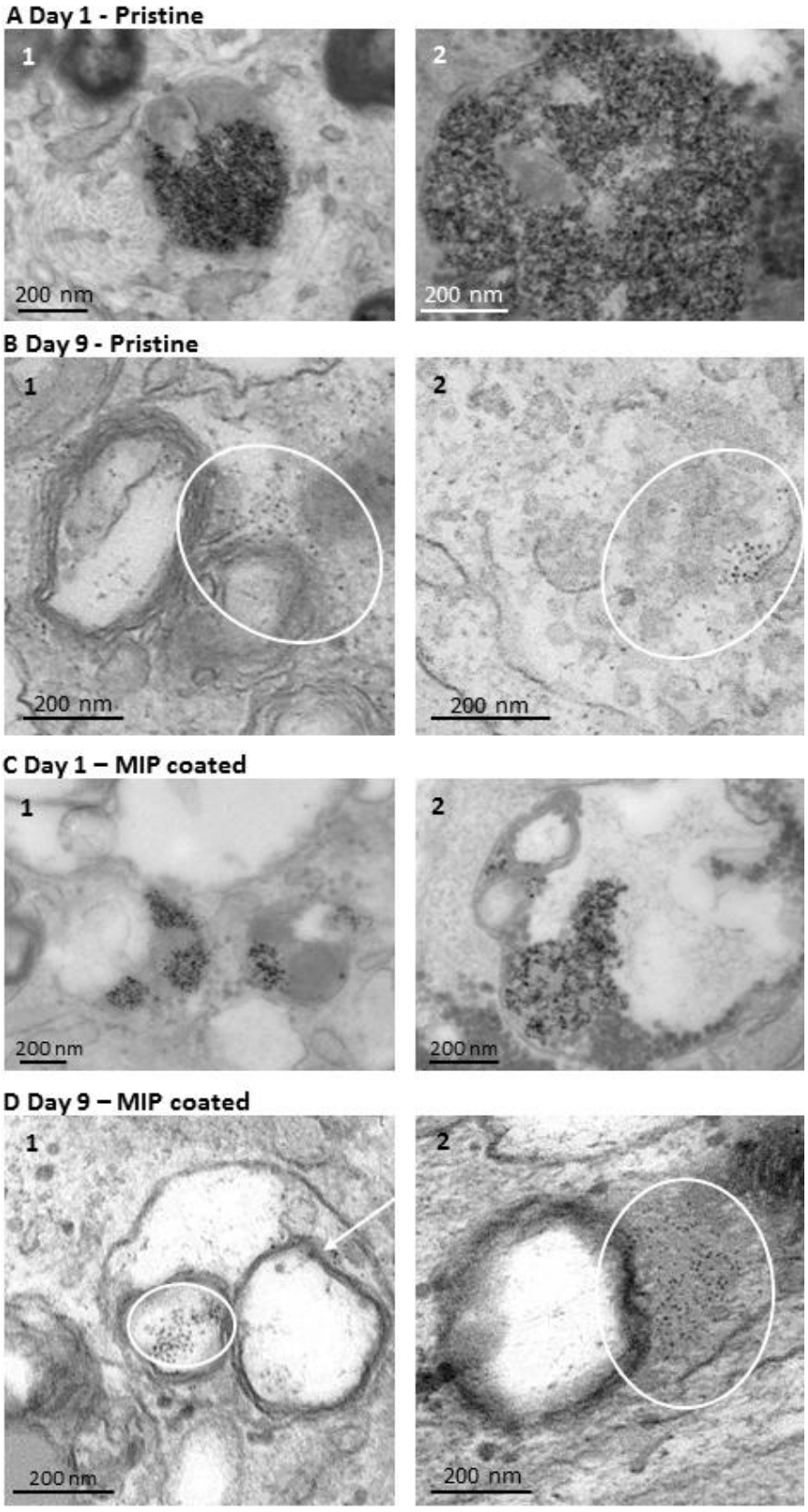

Figure 6: Bare and MIP-coated nanoparticles imaging within the model tissue. (A, B) Transmission electron microscopy of spheroid tissues containing bare maghemite nanoparticles at day 1 (A) and after 9 days of maturation (B). (C, D)

Transmission electron microscopy of spheroid tissues containing γ-Fe_2O_3@MIP hybrid nano-objects at day 1 (C) and after 9 days of maturation (D). At day 1, nanoparticles are confined inside the endosomes (lysosomes) and no dark spots are visible inside the cytoplasm (A, C). While at day 9, some endosomes are still filed with nanoparticles but most of them contain black spots identified as iron-loaded ferritins (see enlarged B2 and D2, white arrows).

Transmission electron microscopy is the technique of choice to track intracellular nanoparticles transformations at the nanoscale. Figure 6 displays TEM images of the tissue containing pristine or MIP-coated maghemite nanoparticles after 1 day (A, C) or 9 days of maturation (B, D; additional images are shown in Figure S5, ESI[†]).

At day 1, all nanoparticles were located within the endosomes. Bare nanoparticles appear to fill almost all the endosomes volume (see enlarged Figure 6 A2), while smaller aggregates embedded inside light gray spots, being the polymer coating, are visible for MIP-coated iron oxides (see Figure 6 C2). At this early day, cytoplasm does not contain any nanoparticles-like objects.

At day 9, only rare maghemite nanoparticles were still detected inside the endosomes, may they be pristine or MIP-coated nanoparticles. On the contrary, a large number of smaller electron-dense and well defined spots appeared within the cytoplasm (see Figure 6, the white arrows on enlarged B2 and D2). These dark nanospots can be identified as iron-loaded ferritins[54–56], and can be found either in the endosomes or in the cytosol. As these spots labelled as loaded-ferritin are missing at day 1, they can be outlined as characteristics of iron oxides degradation. On Figure 6D, one can also observe a contrasted while not well-defined area on the endosome edge, which can be identified as the remaining imprinted polymer.

These observations confirm the important magnetic iron degradation observed macroscopically through magnetic measurements and the storage of the released iron ions by ferritins. Moreover, these iron loaded-proteins being present in both tissues, containing initially bare nanoparticles or hybrid nano-objects, they confirm the possible degradation of magnetic nanoparticles even when they are embedded inside the imprinted polymer.

Conclusion

The long term fate of intracellular magnetic imprinted polymers is still largely unexplored, while these particles are promising tools in nanomedicine, and this knowledge will be imperative before considering clinical applications. Although the future of imprinted polymer inside a biological environment is not elucidated here, we have evidenced for the first time that this coating does not strongly influence maghemite nanoparticles degradation in the long term. The monitoring of iron oxide degradation in a lysosome-like buffer evidenced the potential shielding effect of the polymer coating, but enzymes potentially present in the intracellular compartments modulate it. The polymer coating slows down the degradation process of iron oxide nanoparticles from 9 days for bare nanoparticles to 21 days for the coating ones.

MIP-coated magnetic iron oxide nanoparticles are biocompatible, with a cytotoxicity between 10-15% at the concentrations tested (0.05, 0.1 and 0.2 mM), and are able to undergo cellular internalization as well as pristine nanoparticles. Once inside endosomes, magnetic nanoparticles go through a dissolution inducing a magnetization loss of the model tissue, and an intracellular release of iron-loaded ferritins. Interestingly, polymer coating still seems to potentially slow down the particles degradation without hindering it.

As the nature of the imprinted protein only modify the size and shape of the cavities inside the polymer, the results presented here might be easily applied to other hybrid nano-objects, as could be the monitoring methods employed, when using acrylamide as functional monomer.

Supporting information description

Synthetic procedures and complementary details on materials characterization and degradation *in vitro* and in the spheroid model (Figures S1- S6). This material is available free of charge *via* the Internet at http://pubs.acs.org

Acknowledgements

The authors would like to thank Aude Michel Tourgis and Delphine Talbot, who helped carrying out some characterizations of the materials, as well as Dario Taverna for the high-resolution transmission electron microscopy of the nano-objects. The authors acknowledge the staff of the MBT (physical properties – low temperature) platform of Sorbonne Université for their support.

Conflicts of interest

The authors have no conflict of interest to declare.

References

(1) Butz, K.; Denk, C.; Ullmann, A.; Scheffner, M.; Hoppe-Seyler, F. Induction of Apoptosis in Human Papillomaviruspositive Cancer Cells by Peptide Aptamers Targeting the Viral E6 Oncoprotein. *Proc. Natl. Acad. Sci.* **2000**, *97* (12), 6693–6697. https://doi.org/10.1073/pnas.110538897.

(2) Farokhzad, O. C.; Jon, S.; Khademhosseini, A.; Tran, T.-N. T.; LaVan, D. A.; Langer, R. Nanoparticle-Aptamer Bioconjugates: A New Approach for Targeting Prostate Cancer Cells. *Cancer Res.* **2004**, *64* (21), 7668–7672. https://doi.org/10.1158/0008-5472.CAN-04-2550.

(3) Rothbauer, U.; Zolghadr, K.; Tillib, S.; Nowak, D.; Schermelleh, L.; Gahl, A.; Backmann, N.; Conrath, K.; Muyldermans, S.; Cardoso, M. C.; Leonhardt H. Targeting and Tracing Antigens in Live Cells with Fluorescent Nanobodies. *Nat. Methods* **2006**, *3* (11), 887–889. https://doi.org/10.1038/nmeth953.

(4) Chiu, H.-Y.; Deng, W.; Engelke, H.; Helma, J.; Leonhardt, H.; Bein, T. Intracellular Chromobody Delivery by Mesoporous Silica Nanoparticles for Antigen Targeting and Visualization in Real Time. *Sci. Rep.* **2016**, *6*, 25019. https://doi.org/10.1038/srep25019.

(5) Ghahroudi, M. A.; Desmyter, A.; Wyns, L.; Hamers, R.; Muyldermans, S. Selection and Identification of Single Domain Antibody Fragments from Camel Heavy-Chain Antibodies. *FEBS Lett.* **1997**, *414* (3), 521–526. https://doi.org/10.1016/S0014-5793(97)01062-4.

(6) Vaneycken, I.; Devoogdt, N.; Van Gassen, N.; Vincke, C.; Xavier, C.; Wernery, U.; Muyldermans, S.; Lahoutte, T.; Caveliers, V. Preclinical Screening of Anti-HER2 Nanobodies for Molecular Imaging of Breast Cancer. *FASEB J.* **2011**, *25* (7), 2433–2446. https://doi.org/10.1096/fj.10-180331.

(7) Li, S.; Xu, H.; Ding, H.; Huang, Y.; Cao, X.; Yang, G.; Li, J.; Xie, Z.; Meng, Y.; Li, X.; Zhao Q.; Shen B.; Shao N. Identification of an Aptamer Targeting HnRNP A1 by Tissue Slide-Based SELEX. *J. Pathol.* **2009**, *218* (3), 327–336. https://doi.org/10.1002/path.2543.

(8) Song, K.-M.; Lee, S.; Ban, C.; Song, K.-M.; Lee, S.; Ban, C. Aptamers and Their Biological Applications. *Sensors* **2012**, *12* (1), 612–631. https://doi.org/10.3390/s120100612.

(9) Haupt, K. Imprinted Polymers—Tailor-Made Mimics of Antibodies and Receptors. *Chem. Commun.* **2003**, No. 2, 171–178. https://doi.org/10.1039/b207596b.

(10) Bossi, A.; Bonini, F.; Turner, A. P. F.; Piletsky, S. A. Molecularly Imprinted Polymers for the Recognition of Proteins: The State of the Art. *Biosens. Bioelectron.* **2007**, *22* (6), 1131–1137. https://doi.org/10.1016/j.bios.2006.06.023.

(11) Hua, Z.; Chen, Z.; Li, Y.; Zhao, M. Thermosensitive and Salt-Sensitive Molecularly Imprinted Hydrogel for Bovine Serum Albumin. *Langmuir* **2008**, *24* (11), 5773–5780. https://doi.org/10.1021/la703963f.

(12) Qin, Y.-P.; Jia, C.; He, X.-W.; Li, W.-Y.; Zhang, Y.-K. Thermosensitive Metal Chelation Dual-Template Epitope Imprinting Polymer Using Distillation–Precipitation Polymerization for Simultaneous Recognition of Human Serum Albumin and Transferrin. *ACS Appl. Mater. Interfaces* **2018**. https://doi.org/10.1021/acsami.8b00327.

(13) Canfarotta, F.; Lezina, L.; Guerreiro, A.; Czulak, J.; Petukhov, A.; Daks, A.; Smolinska-Kempisty, K.; Poma, A.; Piletsky, S.; Barlev, N. A. Specific Drug Delivery to Cancer Cells with Double-Imprinted Nanoparticles against Epidermal Growth Factor Receptor. *Nano Lett.* **2018**, *18* (8), 4641–4646. https://doi.org/10.1021/acs.nanolett.7b03206.

(14) Koide, H.; Yoshimatsu, K.; Hoshino, Y.; Lee, S.-H.; Okajima, A.; Ariizumi, S.; Narita, Y.; Yonamine, Y.; Weisman, A. C.; Nishimura, Y.; Oku N.; Miura Y.; Shea K. J. A Polymer Nanoparticle with Engineered Affinity for a Vascular Endothelial Growth Factor (VEGF165). *Nat. Chem.* **2017**, *9* (7), 715–722. https://doi.org/10.1038/nchem.2749.

(15) Griffete, N.; Fresnais, J.; Espinosa, A.; Wilhelm, C.; Bée, A.; Ménager, C. Design of Magnetic Molecularly Imprinted Polymer Nanoparticles for Controlled Release of Doxorubicin under an

Alternative Magnetic Field in Athermal Conditions. *Nanoscale* **2015**, *7* (45), 18891–18896. https://doi.org/10.1039/C5NR06133D.
(16) Dutz, S.; Hergt, R. Magnetic Nanoparticle Heating and Heat Transfer on a Microscale: Basic Principles, Realities and Physical Limitations of Hyperthermia for Tumour Therapy. *Int. J. Hyperthermia* **2013**, *29* (8), 790–800. https://doi.org/10.3109/02656736.2013.822993.
(17) Dias, J. T.; Moros, M.; del Pino, P.; Rivera, S.; Grazú, V.; de la Fuente, J. M. DNA as a Molecular Local Thermal Probe for the Analysis of Magnetic Hyperthermia. *Angew. Chem. Int. Ed.* **2013**, *52* (44), 11526–11529. https://doi.org/10.1002/anie.201305835.
(18) Pouliquen, D.; Le Jeune, J. J.; Perdrisot, R.; Ermias, A.; Jallet, P. Iron Oxide Nanoparticles for Use as an MRI Contrast Agent: Pharmacokinetics and Metabolism. *Magn. Reson. Imaging* **1991**, *9* (3), 275–283. https://doi.org/10.1016/0730-725X(91)90412-F.
(19) Canfarotta, F.; Waters, A.; Sadler, R.; McGill, P.; Guerreiro, A.; Papkovsky, D.; Haupt, K.; Piletsky, S. Biocompatibility and Internalization of Molecularly Imprinted Nanoparticles. *Nano Res.* **2016**, *9* (11), 3463–3477. https://doi.org/10.1007/s12274-016-1222-7.
(20) Cecchini, A.; Raffa, V.; Canfarotta, F.; Signore, G.; Piletsky, S.; MacDonald, M. P.; Cuschieri, A. In Vivo Recognition of Human Vascular Endothelial Growth Factor by Molecularly Imprinted Polymers. *Nano Lett.* **2017**, *17* (4), 2307–2312. https://doi.org/10.1021/acs.nanolett.6b05052.
(21) Hoshino, Y.; Koide, H.; Urakami, T.; Kanazawa, H.; Kodama, T.; Oku, N.; Shea, K. J. Recognition, Neutralization, and Clearance of Target Peptides in the Bloodstream of Living Mice by Molecularly Imprinted Polymer Nanoparticles: A Plastic Antibody. *J. Am. Chem. Soc.* **2010**, *132* (19), 6644–6645. https://doi.org/10.1021/ja102148f.
(22) Weissleder, R.; Stark, D. D.; Engelstad, B. L.; Bacon, B. R.; Compton, C. C.; White, D. L.; Jacobs, P.; Lewis, J. Superparamagnetic Iron Oxide: Pharmacokinetics and Toxicity. *AJR Am. J. Roentgenol.* **1989**, *152* (1), 167–173. https://doi.org/10.2214/ajr.152.1.167.
(23) Briley-Saebo, K.; Bjørnerud, A.; Grant, D.; Ahlstrom, H.; Berg, T.; Kindberg, G. M. Hepatic Cellular Distribution and Degradation of Iron Oxide Nanoparticles Following Single Intravenous Injection in Rats: Implications for Magnetic Resonance Imaging. *Cell Tissue Res.* **2004**, *316* (3), 315–323. https://doi.org/10.1007/s00441-004-0884-8.
(24) Kuhn, D. A.; Vanhecke, D.; Michen, B.; Blank, F.; Gehr, P.; Petri-Fink, A.; Rothen-Rutishauser, B. Different Endocytotic Uptake Mechanisms for Nanoparticles in Epithelial Cells and Macrophages. *Beilstein J. Nanotechnol.* **2014**, *5*, 1625–1636. https://doi.org/10.3762/bjnano.5.174.
(25) Zhao, J.; H. Stenzel, M. Entry of Nanoparticles into Cells: The Importance of Nanoparticle Properties. *Polym. Chem.* **2018**, *9* (3), 259–272. https://doi.org/10.1039/C7PY01603D.
(26) Mazuel, F.; Espinosa, A.; Luciani, N.; Reffay, M.; Le Borgne, R.; Motte, L.; Desboeufs, K.; Michel, A.; Pellegrino, T.; Lalatonne, Y.; Wilhelm C. Massive Intracellular Biodegradation of Iron Oxide Nanoparticles Evidenced Magnetically at Single-Endosome and Tissue Levels. *ACS Nano* **2016**, *10* (8), 7627–7638. https://doi.org/10.1021/acsnano.6b02876.
(27) Walle, A. V. de; Sangnier, A. P.; Abou-Hassan, A.; Curcio, A.; Hémadi, M.; Menguy, N.; Lalatonne, Y.; Luciani, N.; Wilhelm, C. Biosynthesis of Magnetic Nanoparticles from Nano-Degradation Products Revealed in Human Stem Cells. *Proc. Natl. Acad. Sci.* **2019**, *116* (10), 4044–4053. https://doi.org/10.1073/pnas.1816792116.
(28) Boitard, C.; Rollet, A.-L.; Ménager, C.; Griffete, N. Surface-Initiated Synthesis of Bulk-Imprinted Magnetic Polymers for Protein Recognition. *Chem. Commun.* **2017**, *53* (63), 8846–8849. https://doi.org/10.1039/C7CC04284A.
(29) Carr, H. Y.; Purcell, E. M. Effects of Diffusion on Free Precession in Nuclear Magnetic Resonance Experiments. *Phys. Rev.* **1954**, *94* (3), 630–638. https://doi.org/10.1103/PhysRev.94.630.
(30) Meiboom, S.; Gill, D. Modified Spin-Echo Method for Measuring Nuclear Relaxation Times. *Rev. Sci. Instrum.* **1958**, *29* (8), 688–691. https://doi.org/10.1063/1.1716296.
(31) Lévy, M.; Lagarde, F.; Maraloiu, V.-A.; Blanchin, M.-G.; François Gendron; Wilhelm, C.; Gazeau, F. Degradability of Superparamagnetic Nanoparticles in a Model of Intracellular Environment:

Follow-up of Magnetic, Structural and Chemical Properties. *Nanotechnology* **2010**, *21* (39), 395103. https://doi.org/10.1088/0957-4484/21/39/395103.

(32) Levy, M.; Luciani, N.; Alloyeau, D.; Elgrabli, D.; Deveaux, V.; Pechoux, C.; Chat, S.; Wang, G.; Vats, N.; Gendron, F.; Factor C.; Lotersztajn S.; Luciani A.; Wilhelm C.; Gazeau F. Long Term in Vivo Biotransformation of Iron Oxide Nanoparticles. *Biomaterials* **2011**, *32* (16), 3988–3999. https://doi.org/10.1016/j.biomaterials.2011.02.031.

(33) Gu, L.; Fang, R. H.; Sailor, M. J.; Park, J.-H. In Vivo Clearance and Toxicity of Monodisperse Iron Oxide Nanocrystals. *ACS Nano* **2012**, *6* (6), 4947–4954. https://doi.org/10.1021/nn300456z.

(34) Hink, M. A.; Griep, R. A.; Borst, J. W.; Hoek, A. van; Eppink, M. H. M.; Schots, A.; Visser, A. J. W. G. Structural Dynamics of Green Fluorescent Protein Alone and Fused with a Single Chain Fv Protein. *J. Biol. Chem.* **2000**, *275* (23), 17556–17560. https://doi.org/10.1074/jbc.M001348200.

(35) Kan, X.; Zhao, Q.; Shao, D.; Geng, Z.; Wang, Z.; Zhu, J.-J. Preparation and Recognition Properties of Bovine Hemoglobin Magnetic Molecularly Imprinted Polymers. *J. Phys. Chem. B* **2010**, *114* (11), 3999–4004. https://doi.org/10.1021/jp910060c.

(36) Gao, R.; Zhao, S.; Hao, Y.; Zhang, L.; Cui, X.; Liu, D.; Tang, Y. Facile and Green Synthesis of Polysaccharide-Based Magnetic Molecularly Imprinted Nanoparticles for Protein Recognition. *RSC Adv.* **2015**, *5* (107), 88436–88444. https://doi.org/10.1039/C5RA16374A.

(37) Gai, Q.-Q.; Qu, F.; Liu, Z.-J.; Dai, R.-J.; Zhang, Y.-K. Superparamagnetic Lysozyme Surface-Imprinted Polymer Prepared by Atom Transfer Radical Polymerization and Its Application for Protein Separation. *J. Chromatogr. A* **2010**, *1217* (31), 5035–5042. https://doi.org/10.1016/j.chroma.2010.06.001.

(38) Arbab, A. S.; Wilson, L. B.; Ashari, P.; Jordan, E. K.; Lewis, B. K.; Frank, J. A. A Model of Lysosomal Metabolism of Dextran Coated Superparamagnetic Iron Oxide (SPIO) Nanoparticles: Implications for Cellular Magnetic Resonance Imaging. *NMR Biomed.* **2005**, *18* (6), 383–389. https://doi.org/10.1002/nbm.970.

(39) Dos Santos Afonso, M.; Morando, P. J.; Blesa, M. A.; Banwart, S.; Stumm, W. The Reductive Dissolution of Iron Oxides by Ascorbate. *J. Colloid Interface Sci.* **1990**, *138* (1), 74–82. https://doi.org/10.1016/0021-9797(90)90181-M.

(40) Skotland, T.; Sontum, P. C.; Oulie, I. In Vitro Stability Analyses as a Model for Metabolism of Ferromagnetic Particles (Clariscan™), a Contrast Agent for Magnetic Resonance Imaging. *J. Pharm. Biomed. Anal.* **2002**, *28* (2), 323–329. https://doi.org/10.1016/S0731-7085(01)00592-1.

(41) Roch, A.; Muller, R. N.; Gillis, P. Theory of Proton Relaxation Induced by Superparamagnetic Particles. *J. Chem. Phys.* **1999**, *110* (11), 5403–5411. https://doi.org/10.1063/1.478435.

(42) Gossuin, Y.; Gillis, P.; Hocq, A.; Vuong, Q. L.; Roch, A. Magnetic Resonance Relaxation Properties of Superparamagnetic Particles. *Wiley Interdiscip. Rev. Nanomed. Nanobiotechnol.* **2009**, *1* (3), 299–310. https://doi.org/10.1002/wnan.36.

(43) Kruk, D.; Korpała, A.; Taheri, S. M.; Kozłowski, A.; Förster, S.; Rössler, E. A. 1H Relaxation Enhancement Induced by Nanoparticles in Solutions: Influence of Magnetic Properties and Diffusion. *J. Chem. Phys.* **2014**, *140* (17), 174504. https://doi.org/10.1063/1.4871461.

(44) Kimmich, R. *NMR: Tomography, Diffusometry, Relaxometry*; Springer Berlin Heidelberg, 1997.

(45) Rollet, A.-L.; Neveu, S.; Porion, P.; Dupuis, V.; Cherrak, N.; Levitz, P. New Approach for Understanding Experimental NMR Relaxivity Properties of Magnetic Nanoparticles: Focus on Cobalt Ferrite. *Phys. Chem. Chem. Phys.* **2016**, *18* (48), 32981–32991. https://doi.org/10.1039/C6CP06012A.

(46) Fresnais, J.; Ma, Q.; Thai, L.; Porion, P.; Levitz, P.; Rollet, A.-L. NMR Relaxivity of Coated and Non-Coated Size-Sorted Maghemite Nanoparticles. *Mol. Phys.* **2018**, *0* (0), 1–10. https://doi.org/10.1080/00268976.2018.1527410.

(47) Ye, F.; Laurent, S.; Fornara, A.; Astolfi, L.; Qin, J.; Roch, A.; Martini, A.; Toprak, M. S.; Muller, R. N.; Muhammed, M. Uniform Mesoporous Silica Coated Iron Oxide Nanoparticles as a Highly Efficient, Nontoxic MRI T2 Contrast Agent with Tunable Proton Relaxivities. *Contrast Media Mol. Imaging* **2012**, *7* (5), 460–468. https://doi.org/10.1002/cmmi.1473.

(48) Pinho, S. L. C.; Pereira, G. A.; Voisin, P.; Kassem, J.; Bouchaud, V.; Etienne, L.; Peters, J. A.; Carlos, L.; Mornet, S.; Geraldes, C. F. G. C.; Rocha J.; Delville M.-H. Fine Tuning of the Relaxometry of γ-Fe2O3@SiO2 Nanoparticles by Tweaking the Silica Coating Thickness. *ACS Nano* **2010**, *4* (9), 5339–5349. https://doi.org/10.1021/nn101129r.

(49) Kachbi-Khelfallah, S.; Monteil, M.; Cortes-Clerget, M.; Migianu-Griffoni, E.; Pirat, J.-L.; Gager, O.; Deschamp, J.; Lecouvey, M. Towards Potential Nanoparticle Contrast Agents: Synthesis of New Functionalized PEG Bisphosphonates. *Beilstein J. Org. Chem.* **2016**, *12*, 1366–1371. https://doi.org/10.3762/bjoc.12.130.

(50) McCollister, D. D.; Hake, C. L.; Sadek, S. E.; Rowe, V. K. Toxicologic Investigations of Polyacrylamides. *Toxicol. Appl. Pharmacol.* **1965**, *7* (5), 639–651. https://doi.org/10.1016/0041-008X(65)90119-5.

(51) Sjöholm, I.; Edman, P. Acrylic Microspheres in Vivo. I. Distribution and Elimination of Polyacrylamide Microparticles after Intravenous and Intraperitoneal Injection in Mouse and Rat. *J. Pharmacol. Exp. Ther.* **1979**, *211* (3), 656–662.

(52) Mazuel, F.; Espinosa, A.; Radtke, G.; Bugnet, M.; Neveu, S.; Lalatonne, Y.; Botton, G. A.; Abou-Hassan, A.; Wilhelm, C. Magneto-Thermal Metrics Can Mirror the Long-Term Intracellular Fate of Magneto-Plasmonic Nanohybrids and Reveal the Remarkable Shielding Effect of Gold. *Adv. Funct. Mater.* **2017**, *27* (9), 1605997. https://doi.org/10.1002/adfm.201605997.

(53) Espinosa, A.; Curcio, A.; Cabana, S.; Radtke, G.; Bugnet, M.; Kolosnjaj-Tabi, J.; Péchoux, C.; Alvarez-Lorenzo, C.; Botton, G. A.; Silva, A. K. A.; Abou-Hassan A.; Wilhelm C. Intracellular Biodegradation of Ag Nanoparticles, Storage in Ferritin, and Protection by a Au Shell for Enhanced Photothermal Therapy. *ACS Nano* **2018**, *12* (7), 6523–6535. https://doi.org/10.1021/acsnano.8b00482.

(54) Liu, X.; Theil, E. C. Ferritins: Dynamic Management of Biological Iron and Oxygen Chemistry. *Acc. Chem. Res.* **2005**, *38* (3), 167–175. https://doi.org/10.1021/ar0302336.

(55) Lartigue, L.; Alloyeau, D.; Kolosnjaj-Tabi, J.; Javed, Y.; Guardia, P.; Riedinger, A.; Péchoux, C.; Pellegrino, T.; Wilhelm, C.; Gazeau, F. Biodegradation of Iron Oxide Nanocubes: High-Resolution In Situ Monitoring. *ACS Nano* **2013**, *7* (5), 3939–3952. https://doi.org/10.1021/nn305719y.

(56) Gálvez, N.; Fernández, B.; Sánchez, P.; Cuesta, R.; Ceolín, M.; Clemente-León, M.; Trasobares, S.; López-Haro, M.; Calvino, J. J.; Stéphan, O.; Domínguez-Vera J. M. Comparative Structural and Chemical Studies of Ferritin Cores with Gradual Removal of Their Iron Contents. *J. Am. Chem. Soc.* **2008**, *130* (25), 8062–8068. https://doi.org/10.1021/ja800492z.

Abstract graphic

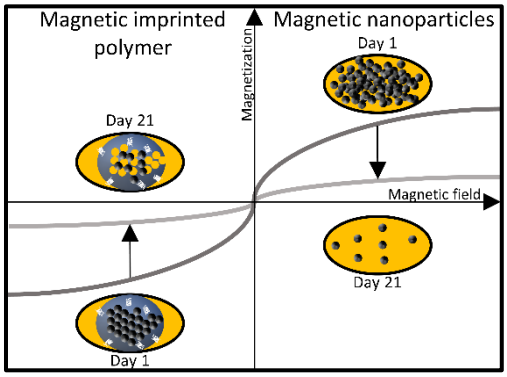

For abstract only.